PC Surface Charge Density from a Vertically Gaussian, Laterally Exposure-Based Volume Charge Distribution in the CGL

Jang Yi and Richard B. Wells
University of Idaho, Moscow, Idaho

Abstract

The surface charge density from a physically plausible volume charge density in the Charge Generation Layer (CGL) is numerically obtained and analyzed. The initial CGL volume charge density is Gaussian in the vertical direction and its lateral variation is obtained from the convolutional laser exposure equations and empirical Photo-Induced Discharge Characteristics (PIDC). The ideal surface charge density without lateral broadening obtained from the PIDC is compared with the resulting charge density after all the holes arrive at the surface. Various Charge Transport Layer (CTL) thicknesses, line widths, and laser spot sizes are used to characterize the effect of these parameters. It is found that the laser spot size has a more significant impact on line broadening than the CTL thickness.

The field dependence of mobility was examined in isotropic materials using a diagonal tensor matrix. The field dependent mobility resulted in submicron line broadening even for a large CTL thickness. Thus line blurring arising from charge transport phenomena is negligibly small in isotropic materials.

Introduction

Charge transport phenomena in photoconductors play a critical role in electrophotographic image resolution. Lateral motion of photogenerated charge carriers during their transit from the CGL to the photoconductor (PC) surface results in line broadening that can ultimately limit the resolvability of thin lines. Line broadening is caused by mutual repulsion of charge carriers. Many attempts have been made to characterize the intrinsic limitation of image resolution. For example, Williams approximated line spreading with a thin charge strip and showed that total broadening of an isolated line (two edges) for a 15 μm layered PC can be as much as 20 μm[1]; Chen calculated the line width as a function of pixel size to PC thickness ratio using a Gaussian surface charge distribution at the CGL/CTL boundary and showed that the line width gets progressively larger as the PC thickness gets larger.[2] In this paper, we incorporate a physically reasonable CGL *volume* charge density in our unipolar charge transport calculation using both field-independent and field-dependent hole mobilities. This volume charge density is Gaussian in the z direction (see Figure 1) and its lateral variation is obtained from the exposure equations and empirical PIDC data.[1,3] The generated holes are injected into the CTL and a set of equations describing the current density, charge density, and electric potential in the PC is solved by a numerical iterative method. The surface charge distribution after all the holes arrive at the PC surface is calculated as several PC and laser parameters are varied.

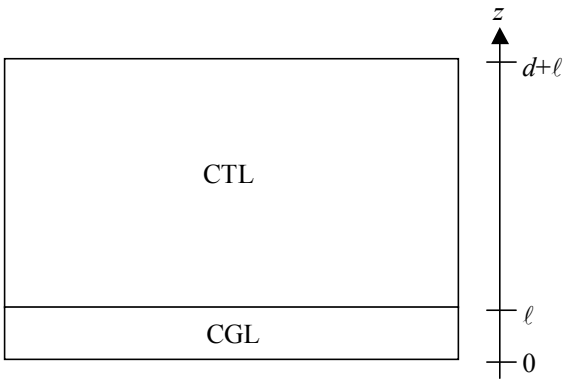

Figure 1. Layered PC

Surface Charge Density without Line Broadening

The coordinate system used in this report is shown in Figure 1. Before exposure, the PC surface is charged with a charge roller to a potential, V_{dark}. The corresponding initial surface charge density is

$$\sigma_0 = \frac{\varepsilon_0 \varepsilon_{PC} V_{dark}}{d + \ell} \tag{1}$$

where d is the CTL thickness, ℓ is the CGL thickness, and ε_{PC} is the dielectric constant of the PC. When the laser beam penetrates the CTL, the generated electrons in the CGL are assumed to neutralize the counter charge in the ground substrate instantaneously while the holes are injected into

the CTL and move toward the surface. The initial volume charge distribution of the holes in the CGL is approximated with

$$\rho(x,y,0 \le z \le \ell, t=0) = \frac{\sigma_{PIDC}(x,y)-\sigma_0}{k_0 \ell} \exp\left(-a_z\left[z-\frac{\ell}{2}\right]^2\right) \quad (2)$$

where k_0 is a calibration factor and a_z is calibrated to yield

$$\exp\left(-a_z(\ell/2)^2\right) = 10^{-5}. \quad (3)$$

$\sigma_{PIDC}(x,y)$ is obtained directly from PIDC data. An example PIDC curve is shown in Figure 2. Typically potential is measured to describe the discharge characteristics of a photoconductor.[3,4] The measured potential is then converted into the corresponding surface charge density using the parallel-plate charge density equation in (1).

In addition to the Gaussian profile in (2), a raised cosine window is applied in the z direction to make the both ends ($z = 0$ and $z = \ell$) go to zero smoothly. The numerator in (2) is the difference between the surface charge density after all the holes arrive at the surface and the surface charge density before the holes are injected into the CTL and hence it represents the quantity of holes generated in the CGL in C/m^2. We convert this surface charge density into the equivalent volume charge density by dividing it by the CGL thickness[1] and an additional conversion factor k_0. k_0 is calibrated by allowing the holes to arrive at the surface and comparing the resultant surface charge density with $\sigma_{PIDC}(x,y)$. It is found that k_0 = 1/3.81 works well for a 26 μm photoconductor with V_{dark} = -600 volts. The equivalent volume charge density in (2) is used as an initial condition when solving for the electric potential and current density in the next section.

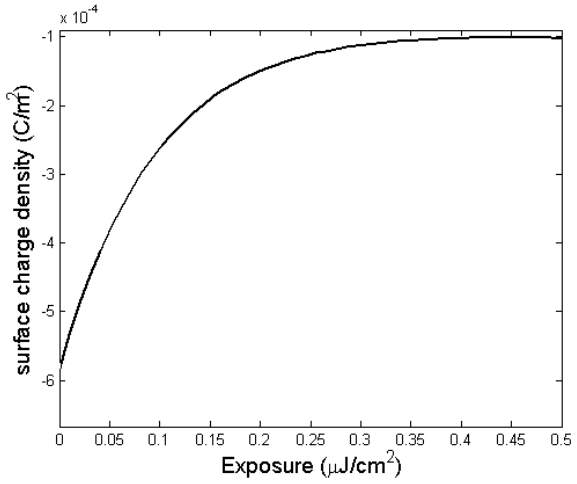

Figure 2. PIDC curve

Surface Charge Density Calculation

The following equations describe the motion of the holes injected into the CTL

$$\frac{\partial^2 V(x,y,z,t)}{\partial x^2}+\frac{\partial^2 V(x,y,z,t)}{\partial y^2}+\frac{\partial^2 V(x,y,z,t)}{\partial z^2} = -\frac{\rho(x,y,z,t)}{\varepsilon_0 \varepsilon_{PC}} \quad (4)$$

$$\mathbf{J}(x,y,z,t) = \rho(x,y,z,t)\boldsymbol{\mu}(x,y,z,t)\mathbf{E}(x,y,z,t) \quad (5)$$

$$\frac{\partial \sigma(x,y,t)}{\partial t} = J_z(x,y,d+\ell,t) \quad (6)$$

$$\frac{\partial \rho(x,y,z,t)}{\partial t} = -\mathrm{div}\mathbf{J}(x,y,z,t) \quad (7)$$

where $\mathbf{J}$ is the current density vector, $\boldsymbol{\mu}$ is the hole mobility tensor, and $\sigma(x, y, t)$ is the time-dependent surface charge density. Just before the holes are injected into the CTL, t = 0 and the volume charge density at $t = 0$ is given in (2). As similarly done by Chen,[2] the differential equations (4)-(7) are written into finite difference equations and the problem is solved by a numerical iterative method. First, the potential at a given time t is obtained from Poisson equation (4) by the iterative relaxation method and the current density is calculated using the negative gradient of the potential. The surface charge density and the volume charge density at a later time $t + \Delta t$ are then calculated from (6) and (7), respectively. This iterative procedure is repeated until all the carriers arrive at the surface. For the sake of calculation efficiency, we eliminated the y variable in these equations by assuming infinitely long lines in the y direction.

Field-Independent Mobility

If we assume the carrier mobility is field-independent, the mobility tensor becomes a constant diagonal matrix

$$\boldsymbol{\mu}(x,y,z,t) = \begin{bmatrix} \mu_x & 0 & 0 \\ 0 & \mu_y & 0 \\ 0 & 0 & \mu_z \end{bmatrix}, \quad (8)$$

where μ_x, μ_y and μ_z are the mobilities in the x, y, and z directions, respectively. Simulation results presented in this section were obtained using a typical mobility of 10^{-6} (cm^2/Vs) in the x and z directions.[5] Figures 3 and 4 show the resulting surface charge density of a single pixel wide line with various CTL thicknesses. The initial volume charge density in the CGL and the initial surface charge density were set to the same values in these simulations. As

previously reported,[2] the line gets thicker as the CTL thickness increases. The horizontal dotted line in Figure 4 is the $1/e^2$ (13.5%) magnitude of the maximum surface charge density, which reveals that a typical PC (20 μm) experiences about one-micron line broadening. Figure 5 shows the total charge in the PC as a function of time. The decay rate becomes smaller as the CTL thickness increases because a thicker PC allows the carriers to spread out more in the CTL.

Figure 6 shows the surface charge density from various line thicknesses while the CTL thickness is fixed at 26 μm. The difference in line broadening in these cases is less than a micron (between 2 μm and 3 μm). As the line thickness increases, the magnitude in the middle approaches that of the ideal surface charge density due to increasing line overlap. The total charge in the PC shown in Figure 7 reveals that the carriers begin to arrive at the surface at the same time; but it takes longer for all of them to reach the surface as the line gets thicker since there are simply more carriers generated in the CGL.

Figure 8 shows the surface charge density of two lines separated by 42 and 62 μm. When they are 62 μm apart, the overlap of line broadening in the middle results in larger surface charge than $\sigma_{PIDC}(x, y)$. Figure 9 shows the normalized surface charge density of a single pixel wide line. Also shown in Figure 9 is the case when the laser spot size and CTL thickness are reduced to one half of their original values, effectively maintaining the same spot size to CTL thickness ratio. More line broadening results from using the half spot size. This is due to the fact that the laser exposure energy is proportional to the laser power and inversely proportional to the spot size. Thus by reducing the spot size while maintaining the same laser power, we effectively increase the horizontal field strength, which in turn causes more line blurring.

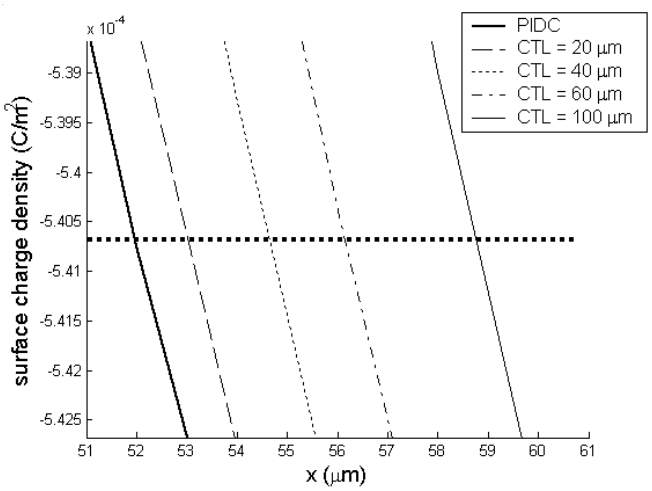

Figure 4. Surface charge density with varying CTL thickness

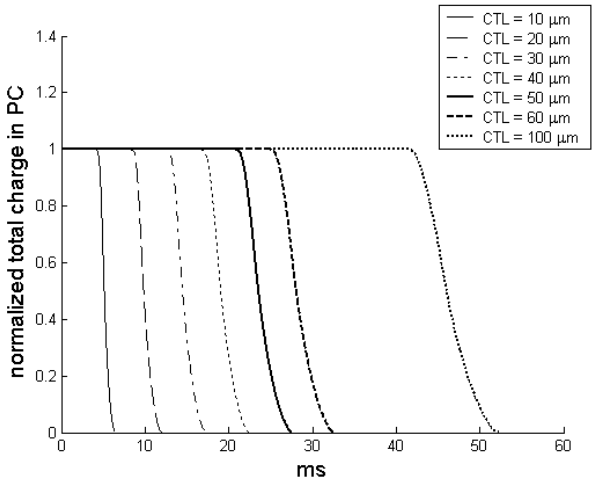

Figure 5.Total charge decay in the PC

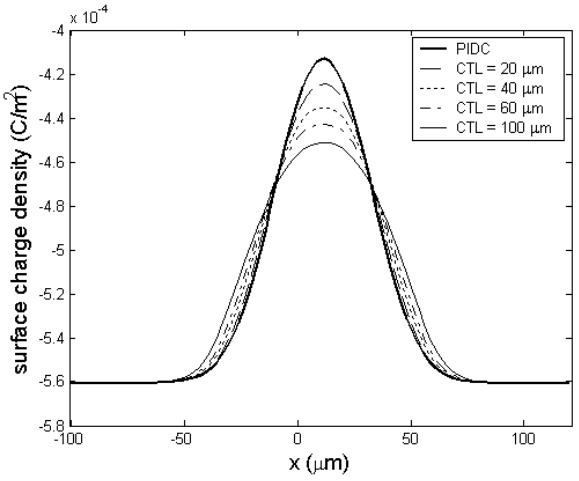

Figure 3. Surface charge density with varying CTL thickness

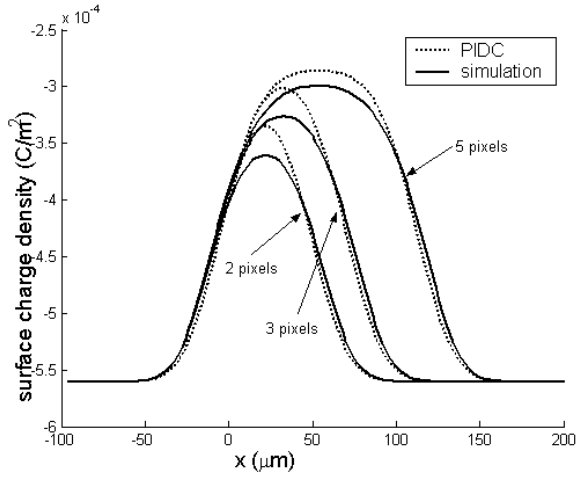

Figure 6. Surface charge density of 2, 3 and 5-pixel wide lines

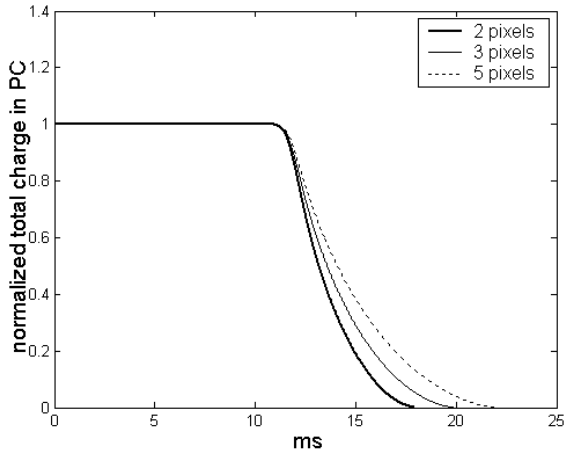

Figure 7. Total charge decay of 2, 3 and 5-pixel wide lines

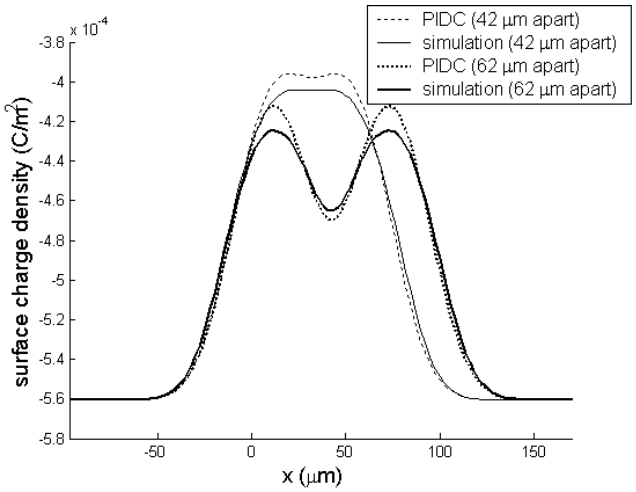

Figure 8. Surface charge density of two lines 42 and 62 μm apart

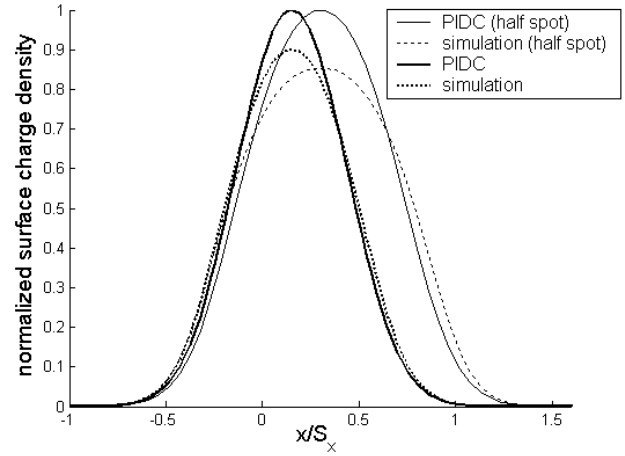

Figure 9. half spot and half CGL thickness

Field-Dependent Mobility

Organic polymeric photoconductors commonly in use today have been known to exhibit a field-dependent conductivity.[5,6] Schein et al. empirically verified that the mobility in a molecularly doped polymer varies exponentially with the square root of electric field,[5] from which we obtain

$$\boldsymbol{\mu}(x,y,z,t) = \begin{bmatrix} \mu_0 e^{a\sqrt{E_x(x,y,z,t)}} & 0 & 0 \\ 0 & \mu_0 e^{a\sqrt{E_y(x,y,z,t)}} & 0 \\ 0 & 0 & \mu_0 e^{a\sqrt{E_z(x,y,z,t)}} \end{bmatrix}, \quad (9)$$

where we used the same curve fit coefficients μ_0 and a that Schein et al. obtained (see Figure 10). Note that we assumed an isotropic material with respect to the field dependence of mobility. That is, carrier movement is independent of spatial directions. For non-isotropic materials, the mobility tensor can be modified accordingly to yield a non-diagonal matrix in a straightforward manner.

Figure 11 shows the surface charge density of a single pixel wide line using (9) and two constant mobility values (1.0×10^{-6} and 3.18×10^{-6} cm^2/Vs). 3.18×10^{-6} cm^2/Vs was obtained from

$$\mu_0 \exp\left(a\sqrt{V_{dark}/(d+\ell)}\right) = 3.18\times10^{-6}\ (cm^2/Vs), \quad (10)$$

When the field dependent mobility is used, the amount of line blurring is negligibly small. Qualitatively speaking, this can be thought of as an amplification of the field effect; if the lateral carrier movement is only a fraction of the vertical transport distance, the field dependent mobility enhances the effect of relatively small horizontal field. Note that the charge density plots using the two fixed mobilities are almost identical. Thus when a constant mobility is used, its value does not affect the resulting line broadening. The charge decay, on the other hand, is very much dependent on the mobility value, as illustrated in Figure 12. Figure 13 shows the charge distribution in the CTL when the mobility is set to 3.18×10^{-6} cm^2/Vs after 1 ms of the initial carrier injection into the CTL, and Figure 14 shows the carriers at the same time when the field dependent mobility is used. Note that the carriers are more spread out with less overall intensity in the latter case. This effectively reduces the repulsion forces among the carriers, which in turn results in less line broadening.

Figure 15 shows the resulting surface charge density when the CTL thickness is 40 μm. Line broadening from the field dependent mobility is still less than 1 μm. Thus it can be concluded that line blurring arising from charge transport phenomena is negligibly small in isotropic materials.

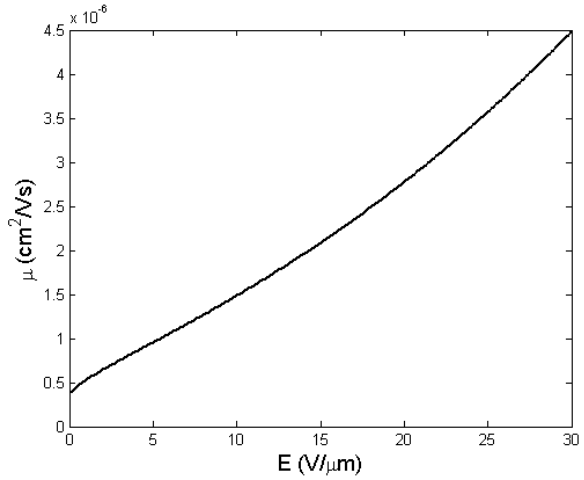

Figure 10.Field dependent mobility[5]

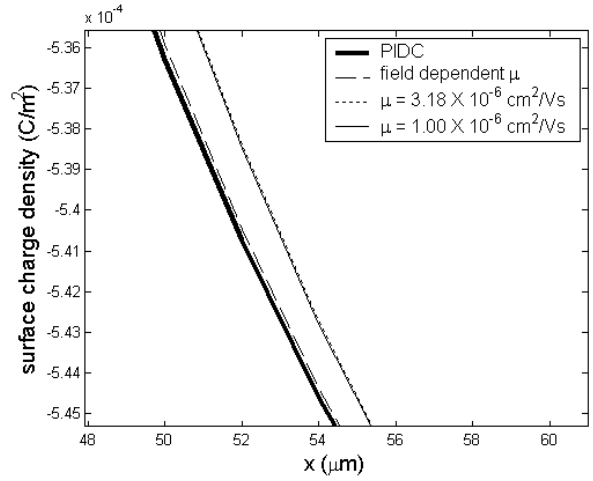

Figure 11. Surface charge densoity using the field dependent mobility (d = 20 μm)

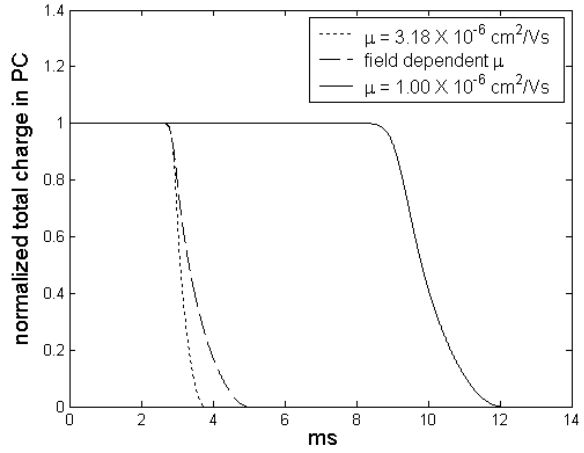

Figure 12. Total charge decay (d = 20 μm)

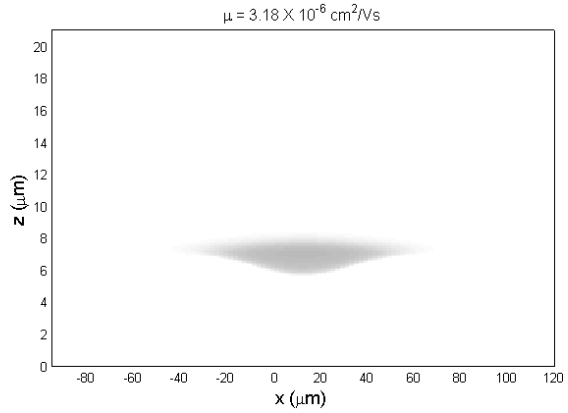

Figure 13. Carrier movement in the CTL using the constant mobility 3.18×10^-6 cm²/Vs (d = 20 μm)

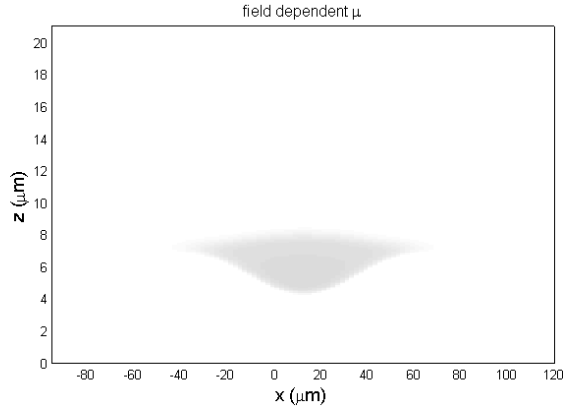

Figure 14. Carrier movement in the CTL using the field dependent mobility (d = 20 μm)

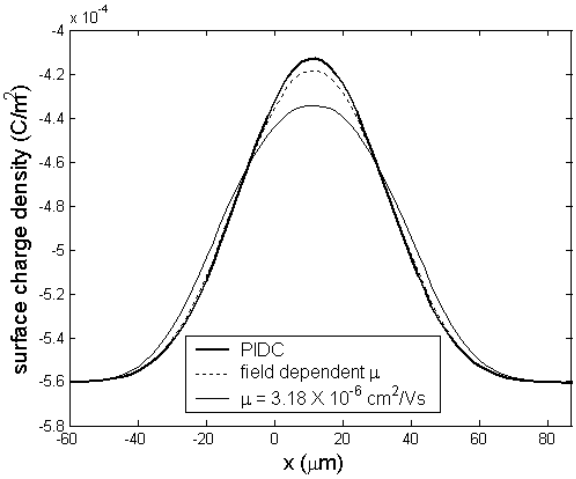

Figure 15. Surface charge density using the field dependent mobility (d = 40 μm)

Acknowledgement

This research was supported by a grant from Hewlett-Packard Company.

References

1. E. M. Williams, *The physics and technology of xerographic processes*, Krieger Publishing Company, Malaba, Florida, 1993
2. I. Chen, Optimization of photoconductors for digital electrophotography, *Journal of Imaging Science* **34**: 15-20 (1990).
3. J. Yi, *A xerographic simulation model*, M.S. thesis, University if Idaho, Moscow ID, May 1999
4. J. Yi et al., Electric Field Calculation based on PIDC in Monocomponent Development Systems, *Proc. NIP-18* pg. 23-27 (2002).
5. L. B. Schein et al., *J. Appl. Phys*., **66**: 686 (1989)
6. D. M. Pai, *J. Appl. Phys*., **46**: 5122 (1975)

Biography

Jang Yi received the B.S. degree in computer engineering in 1997, the M.S. degree in electrical engineering in 1999, and the Ph.D. in electrical engineering in 2002 from the University of Idaho, Moscow, ID. He's currently a research engineer at the same institute. His dissertation was on modeling electrophotographic development physics. His current research area is the development process.